View metadata, citation and similar papers at core.ac.uk

brought to you by CORE

provided by Elsevier - Publisher Connector

HOSTED BY

ELSEVIER

Available online at www.sciencedirect.com

ScienceDirect

Progress in Natural Science: Materials International 25 (2015) 229–235

Progress in Natural Science Materials International

www.elsevier.com/locate/pnsmi
www.sciencedirect.com

Original Research

Effect of thermo-mechanical treatment on mechanical and elastic properties of Ti–36Nb–5Zr alloy

Qingkun Meng[a], Qing Liu[b], Shun Guo[c,*], Yongqi Zhu[a], Xinqing Zhao[a,**]

[a]School of Materials Science and Engineering, Beihang University, Beijing 100191, China
[b]Division of Science and Technology Information, General Research Institute for Nonferrous Metals, Beijing 100088, China
[c]Institute for Advanced Materials, Jiangsu University, Zhenjiang 212013, China

Received 17 November 2014; accepted 16 January 2015
Available online 4 July 2015

Abstract

The evolutions of phase constitutions and mechanical properties of a β-phaseTi–36Nb–5Zr (wt%) alloy during thermo-mechanical treatment were investigated. The alloy consisted of dual (β+α″) phase and exhibited a double yielding phenomenon in solution treated state. After cold rolling and subsequent annealing at 698 K for 20 min, an excellent combination of high strength (833 MPa) and low modulus (46 GPa) was obtained. The high strength can be attributed to high density of dislocations, nanosized α phase and grain refinement. On the other hand, the low Young's modulus originates from the suppression of chemical stabilization of β phase during annealing, which guarantees the low β-phase stability. Furthermore, the single-crystal elastic constants of the annealed Ti–36Nb–5Zr alloy were extracted from polycrystalline alloy using an *in-situ* synchrotron X-ray technique. The results indicated that the low shear modulus C_{44} contributes to the low Young's modulus for the Ti–36Nb–5Zr alloy, suggesting that reducing C_{44} through thermo-mechanical treatment might be an efficient approach to realize low Young's modulus in β-phase Ti alloys. The results achieved in this study could be helpful to elucidate the origin of low modulus and sheds light on developing novel biomedical Ti alloys with both low modulus and high strength.
© 2015 The Authors. Published by Elsevier GmbH. This is an open access article under the CC BY-NC-ND license (http://creativecommons.org/licenses/by-nc-nd/4.0/).

Keywords: Biomedical Ti alloys; Martensitic transformation; Young's modulus; Elastic constants

1. Introduction

Titanium and its alloys have become one of the most attractive classes of biomedical implant materials, because they feature not only excellent biocompatibility, high corrosion resistance and high strength, but also low Young's modulus [1]. For example, the widely used pure Ti and Ti–6Al–4V exhibit low Young's modulus of ~110 GPa, which is only about half that of stainless steel (~206 GPa) and Co–Cr–Mo alloy (~240 GPa) [2]. Compared with α and (α+β) type Ti alloys, the β-phase Ti alloys have even lower modulus. Thus, considerable attention has been paid to develop novel β-phase Ti alloy with low Young's modulus and high strength in the past decades [3]. However, most of the present β-phase Ti alloys perform a modulus ranging from 60 to 80 GPa at an acceptable strength level, which is still higher than that of human bones (~30 GPa) [4]. The large modulus mismatch between implants and human bones could result in so-called "stress shielding effect" and this may lead to bone fracture and loosening of the implants [5]. In order to minimize the "stress shielding effect", Young's modulus of β-phase Ti alloys should be further reduced.

As is well known, Young's modulus of β-phase Ti alloys is closely related to their β-phase stability, i.e., the content of β-stabilizing elements such as Nb, Ta, Mo, etc [6]. The elastic modulus of β-phase decreases monotonically with decreasing β-stabilizing element [7]. As a result, the lowest modulus could be achieved in such a β-phase Ti alloy that contains the least

*Corresponding author. Tel.: +86 511 88783268; fax: +86 511 88797783.
**Corresponding author. Tel.: +86 10 82338559; fax: +86 10 82338200.
E-mail addresses: shunguo@ujs.edu.cn (S. Guo), xinqing@buaa.edu.cn (X. Zhao).
Peer review under responsibility of Chinese Materials Research Society.

http://dx.doi.org/10.1016/j.pnsc.2015.05.001
1002-0071/© 2015 The Authors. Published by Elsevier GmbH. This is an open access article under the CC BY-NC-ND license (http://creativecommons.org/licenses/by-nc-nd/4.0/).

amount of β-stabilizing elements while keeping single β phase [8]. However, a stress-induced martensitic transformation would occur during loading, when the content of β-stabilizing elements is insufficient [9,10]. In such a case, the alloy possesses a very low yield stress although it has a low Young's modulus. Conventional precipitation hardening is not suitable to obtain simultaneously both low modulus and high strength. Because α or/and ω precipitates have much higher modulus than β phase [11]. Thus, the modulus of β-phase Ti alloys could be significantly increased by large amount of precipitates. Furthermore, the precipitation of α or/and ω phases results in a chemical stabilization of the β phase by β-stabilizing element enrichment, which can also increase the elastic modulus of the β phase [12,13]. Recently, a thermo-mechanical treatment including severe cold deformation and subsequent short-time annealing is shown to be an efficient way to strengthen β-phase Ti alloys [14,15]. In this strategy, solute partitioning and the subsequent chemical stabilization of β phase are subtle, which implies that the β phase can keep intrinsically low modulus. On the other hand, the small volume fraction of α or/and ω precipitates contribute little to Young's modulus of the alloys [16]. Therefore, balanced mechanical properties combining high strength and low modulus can be achieved after this kind of thermo-mechanical treatment.

It has been recognized that Young's modulus of a polycrystalline material is determined by its single-crystal elastic constants (SECs) [17]. Therefore, it is helpful to elucidate the origin of low Young's modulus by achieving SECs. However, it is difficult to grow ternary and quaternary β-phase Ti alloy single crystals, and thus the SECs are often difficult or even impossible to obtain. As a result, only few studies were carried out on the elastic properties of β-phase Ti alloys using single crystals. By using *in-situ* synchrotron X-ray diffraction, the lattice strain can be accurately measured during deformation, and the diffraction elastic constants are determined [18–20]. With the aid of an Eshelby–Kroner–Kneer elastoplastic self-consistent (EPSC) model, the SECs can be calculated from the diffraction elastic constants using polycrystalline specimens [21–23].

In this paper, the effect of cold rolling and short-time annealing treatment on the mechanical properties of a β-phase alloy Ti–36Nb–5Zr was investigated (all compositions are given in mass percent unless otherwise stated). Furthermore, the SECs of the Ti–36Nb–5Zr alloy were obtained by using an *in-situ* synchrotron X-ray diffraction technique in order to elucidate the mechanism of the low Young's modulus for the alloy.

2. Experimental

An ingot of Ti–36Nb–5Zr (denoted as Ti-365) was fabricated by arc melting using high purity Ti (99.99%), Nb (99.95%) and Zr (99.95%) as raw materials. The ingot was hot forged to a billet with a cross-section of 8×60 mm^2, and then homogenized at 1223 K for 5 h in vacuum, followed by water quenching. The homogenized billet was cold rolled to a thickness of 1 mm at a reduction of 87.5% (denoted as CR). Part of CR specimens was solution treated at 1073 K for 1 h in an evacuated quartz tube, and quenched into water by breaking quartz tubes (denoted as ST). On the other hand, part of CR specimens was annealed at 523, 623 and 698 K for 20 min, and finally quenched into water.

Uniaxial tensile tests were conducted on an Instron 8801 machine at room temperature with a strain rate of 1×10^{-4} s^{-1}. To ensure the accuracy of Young's modulus, an extensometer was used to measure the strain. All the tensile specimens have a gage length of 30 mm and a cross section of 1×1.46 mm^2. X-ray diffraction (XRD) measurements were performed using a Rigaku D/max2550 diffractometer with Cu Kα radiation. Texture of β phase was measured by a Rigaku D/max-PR diffractometer and the data were processed using popLA [24]. Transmission electron microscopy (TEM) observation was conducted on a FEI Quanta 200F operating at a voltage of 200 kV. *In-situ* uniaxial tensile tests were performed on the beamline 11-ID-C at the Advanced Photon Source, Argonne National Laboratory. High energy monochromatic X-rays have a beam size of 0.4×0.4 mm^2 and a wavelength of 0.10798 Å. The X-ray diffraction rings were segmented and the intensity-lattice spacing diffraction profiles were obtained from a 10° region for grains with crystal plane perpendicular to the loading direction.

3. Results and discussion

3.1. Phase constitutions and mechanical behaviors of the ST and CR alloys

Fig. 1 shows the XRD patterns of the ST and CR Ti-365 alloys. The ST specimen consists of β and α″ martensite, indicating that the β-stabilizing element is not enough to suppress β-to-α″ martensitic transformation during quenching, i.e., the martensitic starting temperature (Ms) is higher than room temperature. Insufficient content of the β-stabilizing element enables the alloy to possess low β-phase stability and guarantees intrinsically low modulus of the β phase. After cold rolling at a reduction of 87.5%, the alloy still exhibits dual (β+α″) phase. Since the XRD patterns are not suitable for accurate quantitative analysis of phase constitution, it is difficult to determine the volume fraction variation of

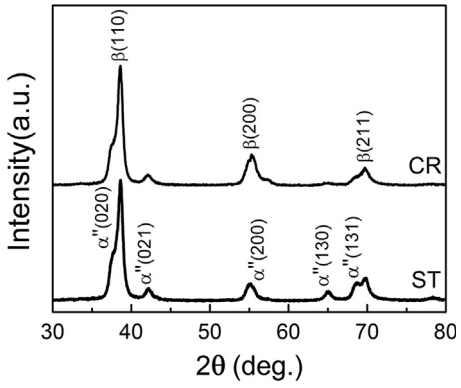

Fig. 1. XRD patterns of the ST and CR alloys.

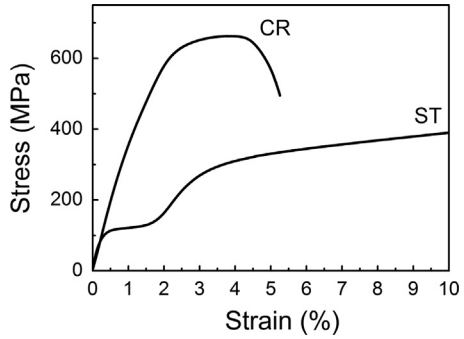

Fig. 2. Tensile stress–strain curves of the ST and CR alloys. Only part of the stress–strain curve from 0% to 10% for the ST alloy is shown.

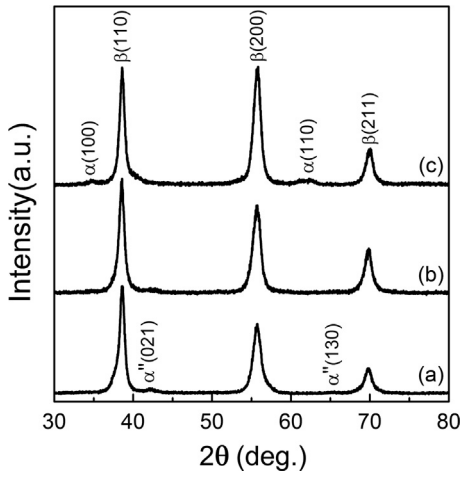

Fig. 3. XRD patterns of the CR alloys annealed at (a) 523 K, (b) 623 K and (c) 698 K for 20 min.

martensite during cold rolling. It was well known that stress-induced martensitic transformation would take place during cold deformation in β-phase Ti alloys with low phase stability [25,26]. Therefore, it is reasonable to believe that the volume fraction of α″ martensite increases after cold rolling because of severe cold deformation.

The stress–strain curves of ST and CR alloy are shown in Fig. 2. The ST alloy exhibits a typical double yielding phenomenon, with the first yielding corresponding to the induction of martensite and the rearrangement of martensite variants, and the second yielding to the initiation of plastic deformation. The first yielding stage enables β-phase Ti alloys to possess functional characteristics such as shape, memory effect and superelasticity [27,28]. However, it is detrimental to the enhancement of strength of the alloys. In order to improve the strength, the stress-induced martensitic transformation during loading should be suppressed. On the other hand, the CR alloy shows peculiar nonlinear deformation behavior. This kind of deformation behavior was frequently reported in metastable β-phase Ti alloys [29,30], and several mechanisms were proposed, such as crystal distortion [31], dislocation loops [32] and giant fault [33]. Recently, studies on CR Ti–25Nb–2Mo–4Sn alloy indicate that the nonlinear deformation behavior could be attributed to stress-induced martensitic transformation [34]. Considering the common nature of the Ti–25Nb–2Mo–4Sn and Ti-365 alloys, i.e., insufficient β-stabilizing element to suppress β-to-α″ martensitic transformation during quenching and experience of severe cold deformation, it is reasonable to believe that the nonlinear deformation behavior of the CR Ti-365 alloy originates from the martensitic transformation during tensile test. Interestingly, Young's modulus decreases from 56 GPa in ST state to 40 GPa after cold rolling. This can be attributed to the formation of $(200)_{\alpha''}$ $[010]_{\alpha''}$ texture and the elastic modulus anisotropy of α″ martensite [35]. Since both β parent phase and α″ martensite contribute to Young's modulus of the ST alloy, it is worth noting that the modulus of β phase in ST state is still at a low level due to the low β-phase stability. Therefore, if the martensitic transformation is suppressed and nearly single β phase is kept to room temperature through thermo-mechanical treatment, high strength and low modulus will be expected to be achieved simultaneously in the present Ti-365 alloy.

3.2. Phase constitutions and mechanical properties of the short-time annealed alloy

As mentioned above, conventional annealing treatment, i.e., long-time annealing at elevated temperature, gives rise to precipitation of large amount of secondary phase and improves the chemical stability of residual β matrix, which makes it impossible to achieve combined properties of high strength and low modulus in β-phase Ti alloys [36]. Therefore, short-time annealing treatment was employed in the present study in an attempt to strengthen the Ti-365 alloy without sacrificing low Young's modulus. Fig. 3 shows the XRD patterns of the CR specimen annealed at 523 K, 623 K and 698 K for 20 min. As indicated in Fig. 3(a), the amount of α″ martensite deceases drastically after annealing at 523 K, implying that the reverse martensitic transformation occurred during the annealing. Stress-induced martensitic transformation during cold deformation and reverse martensitic transformation during subsequent annealing treatment would result in significant grain refinement, which could decrease the Ms temperature [37,38]. Therefore, the martensitic transformation of the Ti-365 alloy was suppressed while quenching from 523 K. As for small amount of residual martensite, two possibilities are as follows, i.e., the incompletion of reverse martensitic transformation during annealing and partial martensitic transformation during quenching. In the present work, it is believed that the residual martensite after short-time annealing treatment originates from the incomplete reverse martensitic transformation and detailed explanation will be discussed later.

After annealing at 623 K, nearly single β phase with a trace of α″ martensite was obtained, as shown in Fig. 3(b). This implies the reverse martensitic transformation was almost completed during annealing. When the annealing temperature was further increased to 698 K, both β phase and α phase were detected from the XRD patterns, while α″ martensite disappeared, as shown in Fig. 3(c). Very weak intensities corresponding to α phase indicates only a very low volume fraction of α precipitated. Moreover, the diffraction angles for β peaks

are not shifted during short-time annealing treatment in comparison with the ST state, implying that the solution partition is subtle. Therefore, the suppression of martensitic transformation in the Ti-365 alloy is attributed to the optimization of microstructures rather than the chemical stabilization of β phase. This is very important for the thermal–mechanical treatment employed in the present study, because it can be postulated that the β phase keeps low phase stability and intrinsically low Young's modulus after annealing treatment.

The tensile stress–strain curves of the CR alloys annealed at 523 K, 623 K and 698 K for 20 min are shown in Fig. 4, and the corresponding Young's modulus, yield stress and ultimate tensile strength are listed in Table 1. Annealing at 523 K significantly increases the strength of the Ti-365, while a quite low Young's modulus of 41 GPa is obtained. The short-time annealing process does not induce the enrichment of β-stabilizing element in residual β matrix, and thus the β phase exhibits a low elastic modulus due to low phase stability. Moreover, low temperature annealing inhibits the precipitation of α and ω phases. These two factors guarantee quite low Young's modulus achieved in the alloy annealed at 523 K. It is worth to point out that double yielding phenomenon does not take place in the annealed alloy, indicating that the β phase is strengthened and the Ms decreases below room temperature. This demonstrates that the small amount of α″ martensite after annealing at 523 K can be ascribed to the incompletion of reverse martensitic transformation. When the annealing temperature is increased to 623 K, the alloy exhibits maximum values of Young's modulus and strength, while possesses worst ductility, which may result from the precipitation of ω phase with high modulus and poor ductility. Although the ω phase is difficult to be detected by XRD when the volume fraction is small, it can exert tremendous influence on the mechanical properties of Ti alloys [39,40]. After annealing at 698 K for 20 min, an excellent combination of low Young's modulus (48 GPa), high strength (833 MPa) and relatively good ductility are achieved, making it a desirable candidate for biomedical applications. It should be pointed out that the alloy annealed at 523 K is not suitable for long-term implant, because it consists of metastable α″ phase. By comparison, the alloy annealed at 698 K is composed of two stable phases in Ti alloy, i.e., β and α phases.

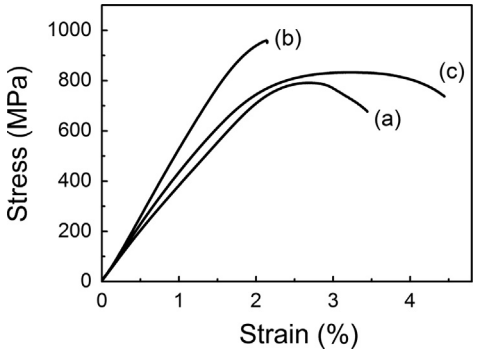

Fig. 4. Tensile stress–strain curves of the CR alloys annealed at (a) 523 K, (b) 623 K and (c) 698 K for 20 min.

Table 1
Young's modulus, yield strength and ultimate tensile strength of the CR alloys annealed at 523, 623 and 698 K for 20 min.

Annealing temperature (K)	Young's modulus (GPa)	Yield strength (MPa)	Ultimate tensile strength (MPa)
523	41	686	790
623	55	912	964
698	46	622	833

Since the alloy annealed at 698 K for 20 min has the balanced properties of high strength and low modulus, TEM observations were carried out to clarify the relationship between mechanical properties and microstructures. The bright-filed micrograph and the corresponding selected area diffraction (SAD) pattern are shown in Fig. 5. It can be seen that nanosized α precipitates are distributed within β matrix, as marked by white arrows. The presence of α phase can be confirmed from the SAD pattern shown in Fig. 5(b), where additional reflections at 1/2{110}β positions are characterized as α phase. In addition, irregular dark area caused by dislocation tangles indicates that the annealed alloy does not undergo complete recrystallization and large amount of dislocations still exists. It has been reported that α phase preferentially nucleates at defects, such as dislocations, grain boundaries and secondary phase [41,42]. In the CR Ti-365 alloy, numerous dislocations induced by cold rolling provide sufficient nucleation sites for the precipitation of α phase. Meanwhile, the growth of precipitates is confined due to the short-time duration in annealing process. As a result,

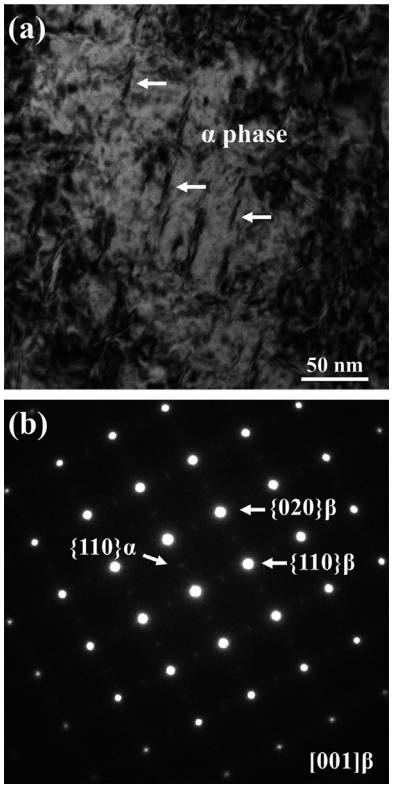

Fig. 5. (a) Bright-filed TEM micrograph of the CR alloy annealed at 698 K for 20 min and (b) the corresponding SAD pattern.

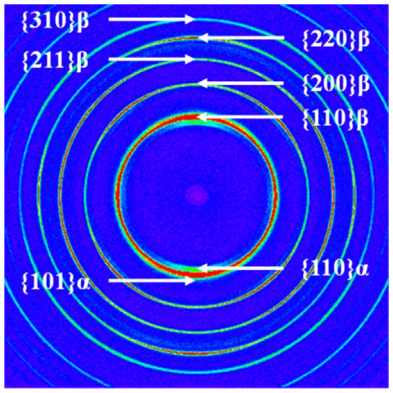

Fig. 6. Two-dimensional synchrotron X-ray diffraction pattern of the CR alloy annealed at 698 K for 20 min.

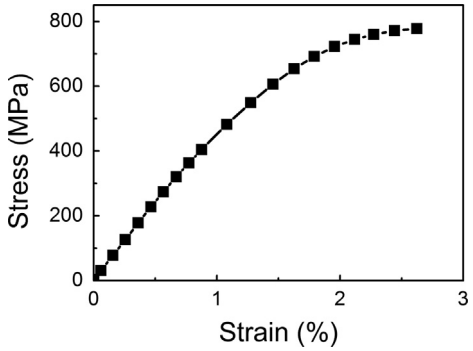

Fig. 7. Tensile stress–strain curves of the CR alloy annealed at 698 K for 20 min obtained during *in-situ* synchrotron X-ray diffraction measurement.

nanometer sized α phase is achieved in the Ti-365 alloy after cold rolling and annealing at 698 K. Previous investigations suggest that in addition to fine α phase, the grain size of β phase can also be significantly reduced by the thermo-mechanical treatment (cold rolling and subsequent short-time annealing) [43,44]. Accordingly, it is concluded that dislocations, nanometer sized α phase and grain refinement enable the Ti-365 alloy to have high strength.

Synchrotron measurement of the 698 K annealed alloy was performed in order to accurately determine the phase constitution, and the two-dimensional synchrotron X-ray diffraction pattern is shown in Fig. 6. The diffraction rings can be indexed as α phase and β phase, and no reflections arising from metastable α″ and ω phases were detected. This agrees well with the XRD and TEM results shown above. In addition, weak intensities of diffraction rings for α phase indicate that the amount of α precipitates is quite small. Thus, this means that the contribution of α phase to Young's modulus is slight, and the β phase with low stability results in low elastic modulus of the annealed alloy.

3.3. Elastic properties of the short-time annealed alloy

The elastic properties of the CR Ti-365 alloy annealed at 698 K for 20 min were investigated using an *in-situ* synchrotron X-ray diffraction technique and an EPSC model. Fig. 7 shows the tensile stress–strain curve obtained during *in-situ* synchrotron X-ray diffraction measurement. The corresponding one-dimensional diffraction patterns for β{110}, {200}, {211} and {310} planes perpendicular to the loading direction are shown in Fig. 8. Upon loading, the β diffraction peaks were initially found shifting to higher *d*-spacing values, implying the elastic deformation. With further increasing the applied stress, the *d*-spacing values tend to be constant, which demonstrates the plastic deformation. When the macrostress is plotted against the lattice strain calculated from Fig. 8 for each β crystal plane, the diffraction elastic constants (DECs) can be measured from the gradient of the macrostress–lattice strain curves. On the other hand, the DECs can be calculated by running EPSC model with SECs as input parameters. It is worth noting that the texture data should be incorporated in the model. Therefore, the EPSC model was performed repeatedly with different SECs and the weighted sum of squared residuals (WSSR) between the measured and calculated DECs were evaluated. When the minimum value of WSSR is obtained, the current SECs input parameters are considered to be representative of the alloy.

As there exist three independent SECs for bcc crystal structure, shear modulus $C'=(C_{11}-C_{12})/2$, shear modulus C_{44} and bulk modulus $K=(C_{11}+2C_{12})/3$ are selected as input parameters for EPSC model in the present study. Compared with the shear moduli C' and C_{44}, it was found the DECs' outputs were insensitive to the bulk modulus. At a given value of K, a set of C' and C_{44} could be used to fit the data with equivalently small WSSR. It is well known that most of β-phase Ti alloys have a bulk modulus value ranging from 100 to 130 GPa [45,46], with few exceptions ranging from 40 to 50 GPa [47,48]. Therefore, the optimum C' and C_{44} were determined by evaluating the WSSR on a grid in C_{44}/C' space at fixed K values of 40 and 120 GPa, respectively. Fig. 9 shows the WSSR for different EPSC inputs. It can be seen that quite a low value of WSSR can be obtained with optimum C', C_{44} and K, which verifies the validity of the present experimentation and modeling. Grid points with minimum-WSSR in Fig. 9, i.e., the elastic parameters of the Ti-365, are listed in Table 2.

According to Hill approximation, Young's modulus of a polycrystalline material is determined by the SECs [17]. In the case of bcc crystal structure, the decrease in C', C_{44} and K would result in the decrease in elastic modulus. It has been well accepted that the shear modulus C' is a direct indicator of β-phase stability, with a low C' corresponding to low β-phase stability [49]. On the other hand, C_{44} and K are independent of β-phase stability. Therefore, the low Young's modulus of most β-phase Ti alloys can be attributed to the low value of C', because of the close relationship between C' and β-phase stability. In order to elucidate the mechanism of the low modulus for the Ti-365 alloy, C', C_{44} and K for three typical β-phase Ti alloys with low modulus, Ti–29Nb–13Ta–4.6Zr [46], Gum Metal [50] and Ti–24Nb–4Zr–8Sn [48], were also listed in Table 2. One can see that all of these three typical β-phase Ti alloys have low C', and Ti–24Nb–4Zr–8Sn has both low C' and K. This indicates that the low C' contributes to low Young's modulus for the Ti–29Nb–13Ta–4.6Zr and Gum

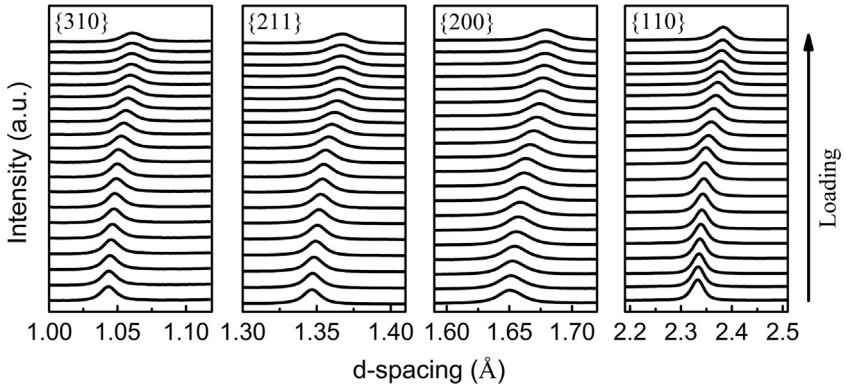

Fig. 8. One-dimensional diffraction patterns recorded in the longitudinal direction at different levels of applied strain for the CR alloy annealed at 698 K for 20 min.

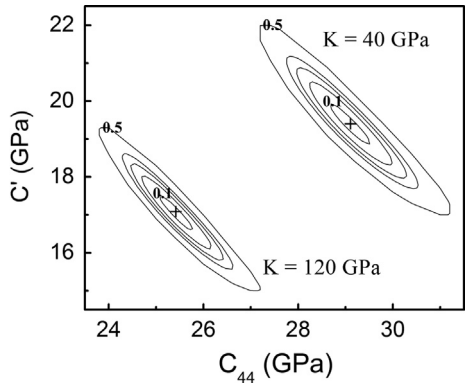

Fig. 9. Contours of WSSR with various EPSC model input parameters.

Table 2
Shear modulus C', shear modulus C_{44} and bulk modulus K for Ti–29Nb–13Ta–4.6Zr (TNTZ), Gum Metal, Ti–24Nb–4Zr–8Sn (Ti-2448) and the present Ti-365 alloy.

Alloy	C' (GPa)	C_{44} (GPa)	K (GPa)
TNTZ	12.9	33.1	111
Gum Metal	14.0	34.1	116
Ti-2448	10.6	35.9	43
Ti-365	19.4	29.1	40
Ti-365	17.1	25.4	120

Metal, while both low C' and low K for the Ti–24Nb–4Zr–8Sn. In sharp contrast, the Ti-365 alloy has relatively higher C' and clearly lower C_{44}, which suggests that C_{44} might also be an important contributor to low Young's modulus. Based on the fact that Ti–29Nb–13Ta–4.6Zr, Gum Metal and Ti–24Nb–4Zr–8Sn consist of single β phase in ST state while the Ti-365 alloy is composed of β and α″, it is proposed that the C_{44} could contribute to low Young's modulus of the alloy for which thermo-mechanical treatment is required to stabilize β phase against α″ martensite.

4. Conclusions

In summary, the effect of thermo-mechanical treatment on the mechanical and elastic properties of Ti-365 alloy was investigated. The ST alloy undergoes martensitic transformation upon cooling and loading, because of low β-phase stability. After cold rolling and annealing at 698 K for 20 min, the microstructure of the alloy is characterized by dominant β phase with a small amount of α phase. Double yielding phenomenon with quite low yield strength was observed in ST state, while balanced properties combining high strength (833 MPa) and low modulus (46 GPa) can be achieved in the annealed alloy. The strengthening of the annealed alloy can be attributed to high density of dislocations, nanosized α precipitates and grain refinement. On the other hand, solution partitioning and chemical stabilization of β phase is limited during short-time annealing treatment, which enables low β-phase stability to be kept after annealing. The SECs' data indicated that the annealed alloy possesses an anomalously low shear modulus C_{44}, which plays an important role in reducing Young's modulus of the Ti-365 alloy.

Acknowledgments

This work was supported by the National Natural Science Foundation of China (Grant nos. 51271010, 51471017, 51431007 and 51401088), the National 973 Program of China (Grant no. 2012CB619403), the China Postdoctoral Science Foundation (2014M561580), the Natural Science Fund for Colleges and Universities in Jiangsu Province (14KJB430007), the Jiangsu Postdoctoral Science Foundation (1401107C) and the Natural Science Foundation of Jiangsu Province (Grant no. BK20140549). The use of the Advanced Photon Source was supported by the US Department of Energy, Office of Science, and Office of Basic Energy Science under Contract no. DE-AC02-06CH11357.

References

[1] M. Long, H.J. Rack, Biomaterials 19 (1998) 1621–1639.
[2] M. Niinomi, Mater. Sci. Eng. A 243 (1998) 231–236.
[3] M. Niinomi, M. Nakai, J. Hieda, Acta Biomater. 8 (2012) 3888–3903.
[4] M. Geetha, A.K. Singh, R. Asokamani, A.K. Gogia, Prog. Mater. Sci. 54 (2009) 397–425.
[5] H.J. Rack, J.I. Qazi, Mater. Sci. Eng. C 26 (2006) 1269–1277.
[6] M. Abdel-Hady, K. Hinoshita, M. Morinaga, Scr. Mater. 55 (2006) 477–480.
[7] A. Biesiekierski, J. Wang, M. Abdel-Hady Gepreel, C. Wen, Acta Biomater. 8 (2012) 1661–1669.

[8] P. Laheurte, F. Prima, A. Eberhardt, T. Gloriant, M. Wary, E. Patoor, J. Mech. Behav. Biomed. Mater. 3 (2010) 565–573.
[9] Y.L. Hao, S.J. Li, S.Y. Sun, R. Yang, Mater. Sci. Eng. A 441 (2006) 112–118.
[10] D.C. Zhang, S. Yang, M. Wei, Y.F. Mao, C.G. Tan, J.G. Lin, J. Mech. Behav. Biomed. Mater. 13 (2012) 156–165.
[11] D. Banerjee, J.C. Williams, Acta Mater. 61 (2013) 844–879.
[12] Y.L. Hao, S.J. Li, S.Y. Sun, C.Y. Zheng, R. Yang, Acta Biomater. 3 (2007) 277–286.
[13] S.L. Raghunathan, A.M. Stapleton, R.J. Dashwood, M. Jackson, D. Dye, Acta Mater. 55 (2007) 6861–6872.
[14] F. Sun, S. Nowak, T. Gloriant, P. Laheurte, A. Eberhardt, F. Prima, Scr. Mater. 63 (2010) 1053–1056.
[15] H.Y. Kim, J.I. Kim, T. Inamura, H. Hosoda, S. Miyazaki, Mater. Sci. Eng. A 438–440 (2006) 839–843.
[16] Q. Meng, S. Guo, Q. Liu, L. Hu, X. Zhao, Prog. Nat. Sci.: Mater. Int. 24 (2014) 157–162.
[17] R. Hill, Proc. Phys. Soc. Sec. A 65 (1952) 349.
[18] R.J. Talling, R.J. Dashwood, M. Jackson, D. Dye, Scr. Mater. 60 (2009) 1000–1003.
[19] J. Zhang, Y. Liu, Y. Ren, Y. Huan, S. Hao, C. Yu, Y. Shao, Y. Ru, D. Jiang, L. Cui, Appl. Phys. Lett. 105 (2014) 041910.
[20] J. Zhang, Y. Liu, Y. Huan, S. Hao, D. Jiang, Y. Ren, Y. Shao, Y. Ru, Z. Wang, L. Cui, Mater. Des. 63 (2014) 460–463.
[21] J.D. Eshelby, Proc. R. Soc. Lond., Ser. A 241 (1957) 376–396.
[22] Q. Meng, S. Guo, X. Ren, H. Xu, X. Zhao, Appl. Phys. Lett. 105 (2014) 131907.
[23] R.J. Talling, R.J. Dashwood, M. Jackson, S. Kuramoto, D. Dye, Scr. Mater. 59 (2008) 669–672.
[24] J.S. Kallend, U.F. Kocks, A.D. Rollett, H.R. Wenk, Mater. Sci. Eng. A 132 (1991) 1–11.
[25] W. Chen, Q. Sun, L. Xiao, J. Sun, Metall. Mater. Trans. A 43 (2012) 316–326.
[26] Y. Yang, G.P. Li, G.M. Cheng, Y.L. Li, K. Yang, Appl. Phys. Lett. 94 (2009) 061901.
[27] H.Y. Kim, Y. Ikehara, J.I. Kim, H. Hosoda, S. Miyazaki, Acta Mater. 54 (2006) 2419–2429.
[28] H.Y. Kim, S. Hashimoto, J.I. Kim, H. Hosoda, S. Miyazaki, Mater. Trans. 45 (2004) 2443–2448.
[29] Y.L. Hao, S.J. Li, S.Y. Sun, C.Y. Zheng, Q.M. Hu, R. Yang, Appl. Phys. Lett. 87 (2005) 091906.
[30] N. Sakaguchi, M. Niinomi, T. Akahori, J. Takeda, H. Toda, Mater. Sci. Eng. C 25 (2005) 363–369.
[31] Y.L. Hao, S.J. Li, B.B. Sun, M.L. Sui, R. Yang, Phys. Rev. Lett. 98 (2007) 216405.
[32] J.P. Cui, Y.L. Hao, S.J. Li, M.L. Sui, D.X. Li, R. Yang, Phys. Rev. Lett. 102 (2009) 045503.
[33] T. Saito, T. Furuta, J.-H. Hwang, S. Kuramoto, K. Nishino, N. Suzuki, R. Chen, A. Yamada, K. Ito, Y. Seno, T. Nonaka, H. Ikehata, N. Nagasako, C. Iwamoto, Y. Ikuhara, T. Sakuma, Science 300 (2003) 464–467.
[34] S. Guo, Q.K. Meng, X.N. Cheng, X.Q. Zhao, J. Mech. Behav. Biomed. Mater. 38 (2014) 26–32.
[35] H. Matsumoto, S. Watanabe, S. Hanada, J. Alloys Compd. 439 (2007) 146–155.
[36] H. Matsumoto, S. Watanabe, S. Hanada, Mater. Trans. 46 (2005) 1070–1078.
[37] M.-H. Cai, C.-Y. Lee, Y.-K. Lee, Scr. Mater. 66 (2012) 606–609.
[38] M.-H. Cai, C.-Y. Lee, S. Kang, Y.-K. Lee, Scr. Mater. 64 (2011) 1098–1101.
[39] Y. Al-Zain, H.Y. Kim, T. Koyano, H. Hosoda, T.H. Nam, S. Miyazaki, Acta Mater. 59 (2011) 1464–1473.
[40] Y. Al-Zain, H.Y. Kim, H. Hosoda, T.H. Nam, S. Miyazaki, Acta Mater. 58 (2010) 4212–4223.
[41] S. Guo, Q. Meng, L. Hu, G. Liao, X. Zhao, H. Xu, J. Alloys Compd. 550 (2013) 35–38.
[42] S. Nag, R. Banerjee, R. Srinivasan, J.Y. Hwang, M. Harper, H.L. Fraser, Acta Mater. 57 (2009) 2136–2147.
[43] F. Sun, Y.L. Hao, J.Y. Zhang, F. Prima, Mater. Sci. Eng. A 528 (2011) 7811–7815.
[44] F. Sun, Y.L. Hao, S. Nowak, T. Gloriant, P. Laheurte, F. Prima, J. Mech. Behav. Biomed. Mater. 4 (2011) 1864–1872.
[45] R. Boyer, G. Welsch, E.W. Collings, Materials Properties Handbook: Titanium Alloys, ASM International, Materials Park, OH, 1994.
[46] M. Tane, S. Akita, T. Nakano, K. Hagihara, Y. Umakoshi, M. Niinomi, H. Mori, H. Nakajima, Acta Mater. 58 (2010) 6790–6798.
[47] M. Tane, S. Akita, T. Nakano, K. Hagihara, Y. Umakoshi, M. Niinomi, H. Nakajima, Acta Mater. 56 (2008) 2856–2863.
[48] Y.W. Zhang, S.J. Li, E.G. Obbard, H. Wang, S.C. Wang, Y.L. Hao, R. Yang, Acta Mater. 59 (2011) 3081–3090.
[49] C. Zener, Phys. Rev. 71 (1947) 846–851.
[50] M. Tane, T. Nakano, S. Kuramoto, M. Hara, M. Niinomi, N. Takesue, T. Yano, H. Nakajima, Acta Mater. 59 (2011) 6975–6988.